THESIS

FABRICATION OF NATURAL AND MAGNETIC SLIPPERY SURFACES

Submitted by

Daniel James Sutherland

School of Biomedical Engineering

In partial fulfillment of the requirements

For the Degree of Master of Science

Colorado State University

Fort Collins, Colorado

Summer 2019

Master's Committee:

Advisor: Arun K. Kota

Ketul Popat
Juyeon Park

ABSTRACT

FABRICATION OF NATURAL AND MAGNETIC SLIPPERY SURFACES

Liquid- infused porous surfaces (LIPS) are a type of low adhesion surfaces. They allow most common solids and liquids to slide off the surface easily. Because of this they are able to reduce the adhesion of food, ice, and even blood platelets to surfaces. As a result, LIPS have applications in reducing food waste, aircraft and powerlines deicing, and hemocompatable implants. However, most LIPS are made of toxic fluorocarbon materials.

In this work, in order to eschew toxic fluorocarbon materials, we designed several LIPS made from natural hemp products. The first is an all-natural LIPS made from hemp fibers, which could help reduce or eliminate liquid food waste. The second is an aluminum LIPS that shows excellent anti-icing and de-icing properties. The third is a titanium nanotube LIPS that allows blood to slide off without impinging or clotting. This surface also shows excellent platelet reduction. Finally, we demonstrated a simple way of replicating this LIPS system on multiple metals including copper and steel.

Further, we demonstrated a simple fabrication of LIPS on top of the fabricated texture atop a magnetic tape. Magnetic tapes are no longer widely used and they are extremely difficult to dispose of. In this magnetic tape-based LIPS, we were able to use an external magnet to manipulate droplets on the surface of the magnetic tape. This can lead to a microfluidic system with a repurposed substrate and precise manipulation of droplets using a magnetic field.

ACKNOWLEGEMENTS

The work presented here was made possible by the direct contributions of Wei Wang, Roberta Maia Sabino, and Breanna Novak. I am extremely thankful for the unerring timeliness and hard work you three showed.

I would also like to thank the other graduate students in our research group. Prem Kantam, Hamed Vahabi for our engaging discussions and your wit, Sanli Movafaghi, Sravanthi Vallabhuneni for always challenging me to come up with bigger better ideas, and Matt Cackovic.

Thank you Dr. Ketul Popat for the contributions your lab made to make this project possible. Finally, I would like to thank my advisor Dr. Kota, who saw something in me. Thank you for all the hours you spent advising me and helping me become a better researcher.

TABLE OF CONTENTS

1. Introduction

Liquid infused porous surfaces (LIPS) have allow water and other aqueous liquids to slide at minimum tilt angles. They have received significant interest in recent years due to their wide applicability in aerospace, naval, medical device, and consumer product industries. This interest is propelled by their ability to self-heal and repel many substances that are difficult for conventional repellant surfaces to repel (e.g. ice, protein, micro-organism, and components of blood). The design criteria and fabrication of natural hemp-based liquid infused porous surfaces are presented in chapter 2. Magnetic control of liquid droplets has been of particular interest in microfluidic applications. Many of these surfaces have focused on the manufacture of new magnetic particle infused thin actuators in order to manipulate droplets in a magnetic field. However, there is a need to repurpose old magnetic-particle infused tapes that are difficult to recycle. Manipulation of droplets on top of a repurposed magnetic tape-based LIPS is presented in chapter 3. Potential further areas of investigation for each topic is presented in chapter 4.

1.1 Wettability

The wettability of a surface is characterized by the contact angle of an incident liquid and the contact angle hysteresis. The wetting behavior of a liquid on a physically smooth, chemically homogeneous surface (Figure 1.1) is fundamentally important because it provides a model system, which can be expanded to incorporate textures and additional liquids. For such a system we describe the wetting behavior via Young's relation[1]:

$$cos\theta = \frac{\gamma_{SV} - \gamma_{SL}}{\gamma_{LV}} \qquad \text{(Eq 1.1)}$$

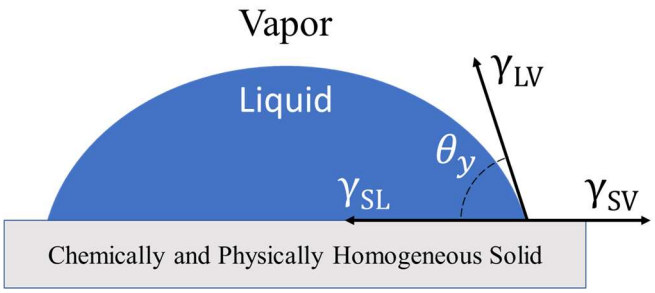

Figure 1.1: *Wetting on a three phase system.*

The γ term represents the energy per unit area between two interfaces. We define *S*, *V*, and *L* as the solid, liquid, and gas phases respectively. Here θ is the equilibrium contact angle. It can be defined as the angle between the tangent to the liquid-vapor interface (γ_{LV}) and the tangent to the liquid-solid interface (γ_{SL}) at the triple phase contact line, measured through the liquid and solid-vapor interface (γ_{SV}). A liquid droplet on a surface with high solid surface energy will tend to spread out (i.e. low contact angle). Whereas on a low solid surface energy surface that same liquid will tend to bead up (i.e. a high contact angle). A surface with a water contact $\theta < 90$ is considered to be hydrophilic, while a surface with $\theta > 90$ is considered to be hydrophobic (Figure 1.2).

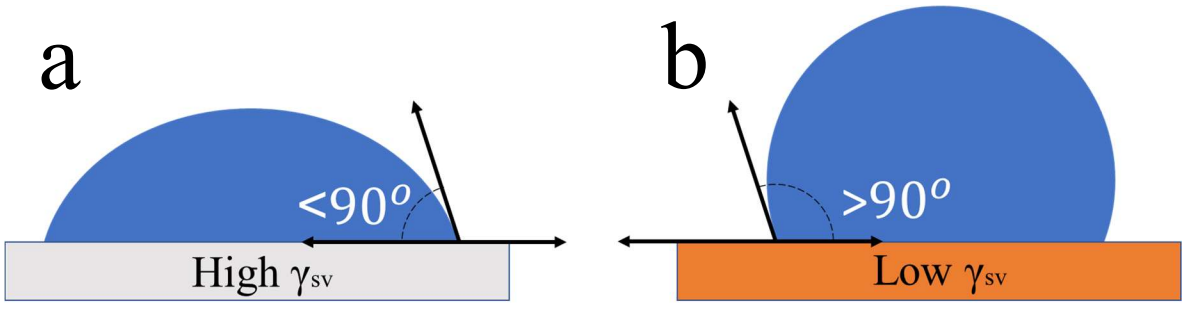

Figure 1.2: *Wetting on a hydrophilic and hydrophobic surface. The droplet is represented in blue. The hydrophilic solid is represented in grey. The hydrophobic solid is represented in orange* ***a)*** *hydrophilic surface.* ***b)*** *hydrophobic surface*

Low surface energy materials are typically non-polar materials, where most molecular interactions come from dispersive interactions. These surfaces are typically composed of long

hydrocarbon chains or perfluorinated carbon chains[2]. High surface energy materials are composed of compounds that contain significant polar interactions; examples of such materials include biological membranes, majority of inorganic minerals such as silicates, hydroxylated oxides, ionic crystals, metallic surfaces[3], and the many polymers[4]. The lowest θ on a flat solid surfaces tend to approach 0°. While the highest θ achievable on a flat surface are typically less than 130°.

The second way to evaluate a surface is via the contact angle hysteresis ($\Delta\theta$)[5]. $\Delta\theta$ is defined as the difference between the advancing (or maximum) contact angle (θ_{adv}) and the receding (or minimum) contact angle (θ_{rec}). Contact angle hysteresis arises from the chemical and physical inhomogeneities of the surface. The advancing and receding contact angles can be measured when a surface is tilted until the droplet just begins to slide. Increase in $\Delta\theta$ results in a increase in sliding angle (ω)[6] and the adhesion of the droplet to the surface. Since a perfectly smooth and chemically homogeneous solid surface is practically impossible, there will always be contact angle hysteresis on solid surfaces. In order to minimize contact angle hysteresis, a liquid-infused[7] surface is required.

1.2 Liquid-Infused Surfaces (LIPS)

A liquid-infused porous surface (LIPS) consists of a porous solid surface infused with a lubricant. Such a LIP surface can allow any liquid immiscible with the lubricant to slide on it with minimal $\Delta\theta$. This is because the lubricant "shields" the immiscible liquid droplet from "experiencing" the inhomogeneities on the solid surface. This is in turn results in relaxation of the no-slip boundary condition, which allows the immiscible liquid droplet to slip (or easily slide) past the surface[8,9].

LIP surfaces are based on the liquid trapping properties of the *Nepenthes* pitcher plant (Figure 1.3). The pitcher plant traps a thin layer of water in the microstructure of peristome. This water acts as a lethal lubricant, forcing any insects that touch the plant to fall into the pitcher. Typically, bio-inspired LIPS trap a low surface tension liquid within the porous matrix of a low surface energy solid.

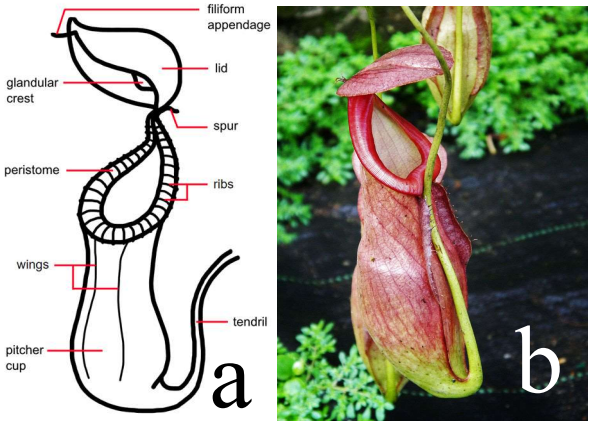

Figure 1.3: *Nepenthes pitcher plant.* ***a)*** *shows the anatomy of the pitcher plant. LIPS are modeled after the properties of the peristome.* ***b)*** *A photograph of the pitcher plant.*

Necessary conditions for LIPS are:

(i) Liquid placed on a LIPS must be immiscible in the lubricant (e.g the droplet is water and the lubricant is an oil).

(ii) The lubricant must spontaneously wet the solid texture.

(iii) The surface must be textured on the micro and/or nano-scale.

(iv) The lubricant must be more compatible with the solid texture than the solid is to the water.

(v) (v) the lubricant should not cloak the droplet.

The possible wetting states of a four-phase system consisting of air (A), a droplet (W), an immiscible lubricant(O), and a textured solid (S) are shown in Figure 1.4.

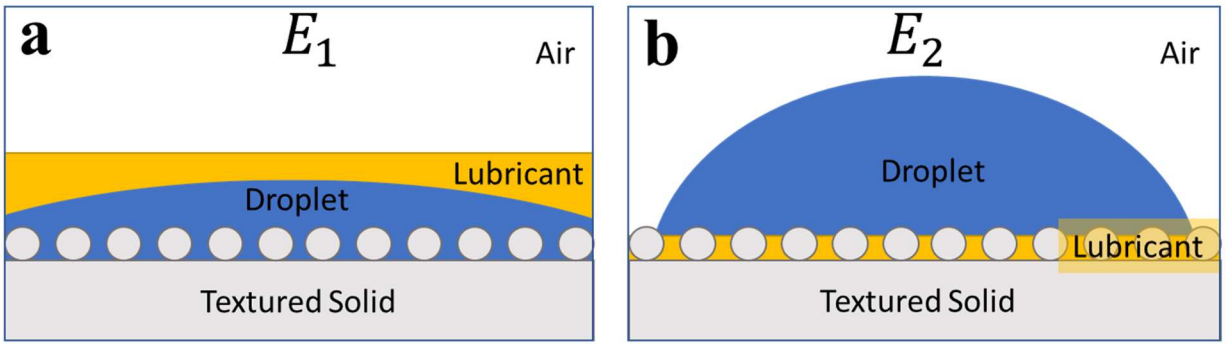

Figure 1.4: *Possible wetting states on a LIP surface. The white area is the air. The yellow area represents the lubricant. Blue represents the droplet, and grey represents the solid texture.* ***a)*** *State E_1, where the droplet displaces the lubricant and wets the texture.* ***b)*** *Shows state E_2, where the droplet rests on top of a composite solid-lubricant interface.*

Of the two possible wetting states, the one with the lowest energy per unit area is the one that will be spontaneously formed[10]. If $E_1 < E_2$ the droplet completely wets solid surface and displaces any lubricant present. In this case, the droplet would pin and fail to slide. If $E_2 < E_1$ the droplet rests on top of composite oil-solid layer. This is the most desirable state for LIP surfaces because the lubricant can be trapped via capillary forces and is more difficult to dislodge[9].

Finally, the droplet should not be cloaked by the lubricant. Cloaking is where lubricant spreads completely over the outside of the droplet (Figure 1.5).

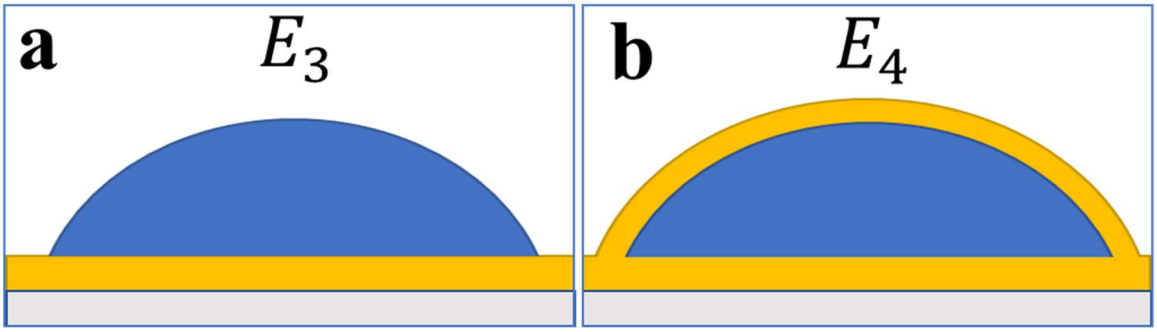

Figure 1.5: *Cloaking on a LIP surface. The white area is the air. The yellow area represents the lubricant. Blue represents the droplet, and grey represents the solid texture.* ***a)*** *State E_3, where the droplet rests on top of the lubricant layer.* ***b)*** *Shows state E_4, where the droplet is cloaked by the lubricant.*

Cloaking is an inherent property of the lubricant and liquid and is independent of the solid texture[11]. If $E_4 < E_3$the lubricant forms a layer over the droplet. This is not desirable as the removal of any droplet, regardless of any other property of the LIPS, will cause the depletion of the lubricant. If $E_3 < E_4$ the droplet will not cloak.

2. All-Natural Slippery Surfaces

2.1 Introduction

There are many reasons to reduce the adhesion of solids and liquids to a surface. Low adhesive surfaces are capable of decreasing food waste accumulation[12], marine anti-fouling[13], corrosion[14], icing[7,15,16], microbial film formation[13,17,18], and platelet adhesion[19]. One strategy to reduce the adhesion is to fabricate a liquid-infused porous surface (LIPS). These surfaces are fabricated through a combination of surface texture, chemical modification, and a lubricant[7]. They can reduce the adhesion of solids and liquids by forcing them to interact with a trapped lubricant layer as opposed to the solid texture[7]. Necessary conditions for LIPS include: (i) liquid placed on a LIPS must be immiscible in the lubricant (e.g droplet is water and lubricant is oil), (ii) the lubricant must spontaneously wet the solid texture. (iii) The surface must be textured on the micro or nano-scale, (iv) the lubricant must be more compatible with the solid texture than the solid is to the water, and (v) the lubricant should not cloak the droplet..[7]

Despite the biological origins of LIPS, they typically are manufactured using synthetic fluorocarbon lubricants and textures (e.g. porous Teflon), which possess extremely low surface tensions (<15 mN m^{-1}) and are immiscible with aqueous liquids. The U.S. Environmental Protection Agency (EPA) classifies long-chain fluorocarbon materials as "emerging contaminants" because of their potential decomposition into perfluorooctanoic acid (PFOA)[20], which is considered environmentally persistent, bio-accumulative, and toxic to humans. Therefore, LIPS coatings fabricated using fluorocarbon materials are not ideal for contacting food, blood, or any application where they might be released into the environment[21].

While many LIPS are omniphobic (i.e., can repel almost all liquids), this is not a necessary condition for many applications of interest. Many liquid repelling applications that involve LIPS surfaces are mostly interacting with aqueous fluids[13,17-19,22-25]. There are very few reports of LIPS fabricated with biodegradable and/or natural materials[19]. The ideal lubricants for a LIP surface should be naturally abundant, easily applied, minimally processed, and preferably biocompatible and biodegradable. This way the LIPS can not only help minimize liquid adhesion but will also not contribute to non-biodegradable waste. To the best of our knowledge, there are no reports of LIPS fabricated with minimally processed, abundant, biodegradable, and biocompatible materials.

For this purpose, we chose hemp oil and fiber as the basis for our LIPS. The hemp crop has low water requirements, low pesticide requirement, and has high yield[26]. Hemp derivatives are used in foods[27], beverages, personal care products, nutritional supplements, fabrics, textiles[28], paper, construction materials, and other manufactured goods[29]. Hemp oils are also an excellent source of essential fatty acids (e.g linoleic acid)[30]. In this work, we used hemp oil and beeswax to easily fabricate a LIPS that aqueous foods (e.g., Honey, Gatorade, Coca- Cola, milk, and syrups) barely adhere to. Further, we evaluated the efficacy of our LIPS surfaces in deicing and reduction of blood platelet adhesion.

2.2 Materials and Characterizations

Hemp paper was purchased from Hemp Traders. Beeswax was purchased from S. C. Johnson, Inc . Hemp oil was purchased from Hemp Traders. Aluminum, copper plates, steel plate, and titanium were purchased from McMaster. Hydrochloric acid, acetone, ethanol, sodium hydroxide, sodium carbonate, iron (III) chloride, hydrofluoric acid, toluene, and propylene glycol were purchased from Sigma Aldrich.

2.2.1 Contact Angles Measurements

Advancing contact angle (θ_{adv}), receding contact angle (θ_{rec}), sliding angles (ω) and surface tension measurements were conducted using a goniometer and tensiometer (Ramé-Hart 260-F4). For non-lubricated surfaces θ_{adv} and θ_{rec} were measured using a 2mL syringe. For lubricated surfaces the stage was tilted and θ_{adv} and θ_{rec} were measured at the angle where the droplet just began to slide (ω). For all lubricated surfaces the θ_{adv}, θ_{rec}, and ω are all representative of the mean of at least three measurements.

The tensiometer was used to determine the surface tension of hemp oil. Ten trials for hemp oil were conducted. Hemp oil's surface tension was determined to be $\gamma_{ov} = 32.8$mN m^{-1}. Because of its low surface energy, hemp oil is assumed to be able to wet a texture satisfying criteria (ii).

2.2.2 Scanning Electron Microscopy

The morphology of the surface was characterized using an SEM (scanning electron microscope). Images were taken with a JEOL-6500F SEM at 15 kV at a working distance of 9.8 mm.

2.2.3 De-icing

The de-icing procedure reported here is a modification of the one used in Beemer *et al*[31] (Figure 2.1). All deicing measurements reported in this paper were done in a -20°C walk-in freezer including the application of shear force to emulate real world conditions as closely as possible. The back of the LIP surface was adhered to a plate that was attached to a rack in the freezer using double sided tape (3M). The plate was fixed with three-pronged clamps. The surface was placed in the freezer for roughly 30 minutes until it equilibrated at -20°C. A square plastic cuvette with cross section 1 cm x 1 cm was placed atop the relevant LIPS. This cuvette

was filled with 0.5 mL prechilled deionized (DI) water (<10ºC). The surface and cuvette were left undisturbed for at least 30 minutes[31].

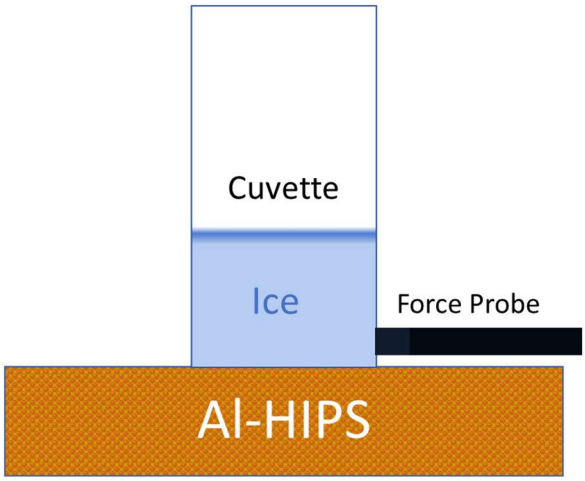

Figure 2.1: *Deicing setup. The cuvette is place on top of the LIP surface. It is filled with 0.5 mL of water and frozen at -20ºC. A force probe is applied at the base of the cuvette.*

A force gauge was attached via a long steel bar to a horizontal plastic probe approximately 2 cm wide with a flat, narrow taper at the end. The force gauge and attachments were then mounted on a linear transition stage. A shear force at a rate of 0.8 mm/s was applied to the base of the frozen cuvettes. The peak force required to remove the frozen cuvette was recorded by the force gauge. Multiple trials (8) were conducted at different locations (2) of the LIP surfaces.

2.2.4 Blood Platelet Adhesion

The adhesion of platelets to the relevant LIP surface were evaluated using a modified procedure from Movafaghi *et al*[32]. Whole blood was drawn from a healthy individual with care to avoid locally activated platelets. Blood was centrifuged in vials at 300 g for 15 min to separate the human blood plasma. Sterilized relevant LIP surfaces (irradiated under UV for at least 30 minutes) were incubated in 1 mL of the plasma in a 24 well plate at 37 °C and 5% CO2 on a horizontal shaker plate (100 rpm) for 2 h.

After incubation of relevant LIP surfaces in human blood plasma, the unadhered platelets were removed by gently rinsing with PBS. Adhered platelets were fixed in a 3.7 wt% formaldehyde in PBS solution for 15 min and subsequently washed multiple times with PBS. The cell membranes were permeabilized using 1% Triton X in PBS for 3 min. The LIP surfaces were then incubated in PBS solutions containing 500 µL of rhodamine phalloidin (cytoskeleton red stain) for 25 min. The surfaces were subsequently rinsed with PBS and imaged using a fluorescence microscope (Zeiss). The % area of adhered platelets was obtained using ImageJ software.

2.2.5 Owens-Wendt Analysis

The equilibrium configuration of a liquid drop on a smooth solid surface is given by the Young's equation[1] as:

$$cos\theta = \frac{\gamma_{SV} - \gamma_{SL}}{\gamma_{LV}} \quad \text{(Eq 2.1)}$$

Of the four parameters in Eq. 2.1, the liquid surface tension γ_{lv} and the equilibrium contact angle θ are readily measurable. In order to determine both the solid surface energy γ_{SV} and the solid-liquid interfacial energy γ_{SL} another relationship between γ_{SV} and γ_{SL} is required. Typically, this additional relationship is obtained from an equation of state approach or a surface energy component approach. We adopted the surface energy component approach prescribed by Owens and Wendt[33] to estimate γ_{sv} According to this approach, the solid surface energy is the sum of contributions from two types of intermolecular forces at the surface:

$$\gamma_{sv} = \gamma_{sv}^{d} + \gamma_{sv}^{p} \quad \text{(Eq. 2.2)}$$

Here γ_{sv}^{d} is the component that accounts for the dispersive forces, while γ_{sv}^{p} is the component that accounts for the polar forces, such as hydrogen bonding. Further, this approach postulates that:

$$\gamma_{SL} = \gamma_{SV} + \gamma_{LV} - 2\left(\sqrt{\gamma_{LV}^{d}\gamma_{SV}^{d}} + \sqrt{\gamma_{LV}^{p}\gamma_{SV}^{p}}\right) \quad \text{(Eq. 2.3)}$$

Here, γ_{LV}^{d} and γ_{LV}^{p} are the dispersive and polar components of the liquid surface tension, respectively. Combining Eqs. 2.2-2.3 and recognizing that the polar component of liquid surface tension is zero ($\gamma_{LV}^{p} = 0$) for non-polar liquids such as oils, the dispersive component of solid surface energy is given as:

$$\gamma_{sv}^{d} = \gamma_{LV}\left(\frac{1+\cos\theta}{2}\right)^{2} \quad \text{(Eq 2.4)}$$

In Eq. 2.4, γ_{LV} is the surface tension of a non-polar liquid and θ is the equilibrium contact angle of the same non-polar liquid on the solid surface. We used rapeseed oil (γ_{lv} = 35.7mN m^{-1}) as the non-polar liquid to estimate γ_{SV}^{d}. After determining the dispersive component γ_{SV}^{d}, combining Eqs. 2.2 and 2.3 for a polar liquid ($\gamma_{LV}^{p} \neq 0$), the polar component of the solid surface energy is given as:

$$\gamma_{SV}^{p} = \frac{1}{\gamma_{LV}^{p}}\left[\frac{\gamma_{LV}(1+\cos\theta)}{2} - \sqrt{\gamma_{LV}^{d}\gamma_{SV}^{d}}\right]^{2} \quad \text{(Eq. 2.5)}$$

In Eq. 2.5 γ_{LV} is the surface tension of a polar liquid and θ is the equilibrium contact angle for the same polar liquid on the solid surface. We used water (γ_{LV}^{d}= 21.1 mN m^{-1} and γ_{LV}^{p} = 51.0 mN m^{-1}) as the polar liquid to estimate γ_{SV}^{p}.

The various interfacial energies γ_{sw}, γ_{so}, and γ_{wo} were further calculated using this Owens-Went analysis[33]. The subscripts correspond to the phase: solid (S), lubricant (O), aqueous (W), and vapor (V). γ_{sw} denotes the interfacial energy of the solid being wet by water. γ_{so} is the interfacial energy of the solid being wet by the lubricant. γ_{wo} is the interfacial tension between the lubricant and water. The solid phase (S) is either cellulose (γ_{LV}^{d}= 27.5 mN m^{-1} and γ_{LV}^{p} = 41.0 mN m^{-1})[34] or beeswax (γ_{LV}^{d}= 27.4 mN m^{-1} and γ_{LV}^{p} = 0.2 mN m^{-1})[35] The lubricant (O) is hemp oil

(γ_{LV}^{d}= 32.8 mN m^{-1} and γ_{LV}^{p} = 0 mN m^{-1}) as previously determined by tensiometer. The following equations were used to determine γ_{sw}, γ_{so}, and γ_{wo}. The results are shown in Table 2.2.

$$\gamma_{sw} \approx \gamma_{sv} + \gamma_{wv} - 2\left(\sqrt{\gamma_{wv}^{d}\gamma_{sv}^{d}} + \sqrt{\gamma_{wv}^{p}\gamma_{sv}^{p}}\right) \quad \text{(Eq. 2.6)}$$

$$\gamma_{wo} \approx \gamma_{wv} + \gamma_{ov} - 2\left(\sqrt{\gamma_{wv}^{d}\gamma_{ov}^{d}}\right) \quad \text{(Eq. 2.7)}$$

$$\gamma_{so} \approx \gamma_{sv} + \gamma_{ov} - 2\left(\sqrt{\gamma_{wv}^{d}\gamma_{so}^{d}}\right) \quad \text{(Eq. 2.8)}$$

Table 2.2*: The calculated interfacial energies for each of the phases on both beeswax and cellulose fibers.*

Interface	Interfacial Energy (mJ m^{-2})	
	Cellulose (Hydrophilic)	Cellulose Coated Beeswax (Hydrophobic)
γ_{sw}	0.2	40.5
γ_{so}	41.2	0.5
γ_{wo}	46.7	46.7

2.3 Designing a LIP surface

Macroscopic and SEM imagining reveal that hemp paper is porous on the macro (Figure 2.2a) and micro scales (Figure 2.2b-c). We chose this material to satisfy condition (iii).

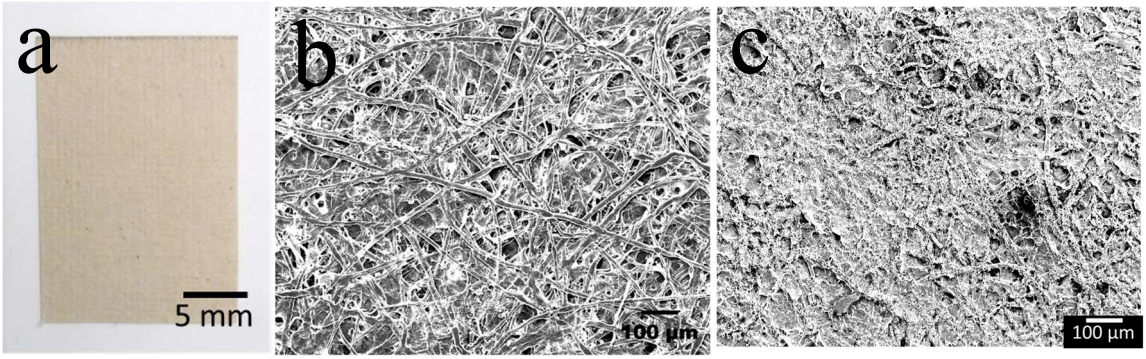

Figure 2.2*: **a)** Visible roughness of hemp paper at 5mm.* ***b)*** *SEM of hemp paper showing random orientation of cellulose fibers.* ***c)*** *SEM of hemp paper coated with 150 mg mL $^{-1}$ beeswax*

The wetting state of a liquid droplet on top of a textured lubricated surface can be characterized by the relative position of the three materials: the solid, lubricant, and liquid. Where these are in relation to one another determines whether a droplet will slide easily or be pinned in the texture. There are two possible wetting states. The first E_1 is defined as the droplet displacing the lubricant and pinning in the texture. This state has high adhesion and is not desired for LIP surface. The second state E_2 is defined as the droplet resting on top of a combination of the solid and lubricant. This state has minimal adhesion and is desired for LIPS. Whichever state has the lower energy per unit area will spontaneously occur on the surface. The equilibrium position of each of these states is determined by the following[10]:

$$E_1 = r * \gamma_{sw} \qquad \text{(Eq. 2.9)}$$

E_1 is the energy per unit area of the aqueous droplet wetting the entire texture and displacing the lubricant. γ_{sw} is the energy per unit area between water and the solid. r is the texture dependent roughness factor. It is defined as the total area of the solid liquid interface

divided by the projected area of the solid liquid interface.

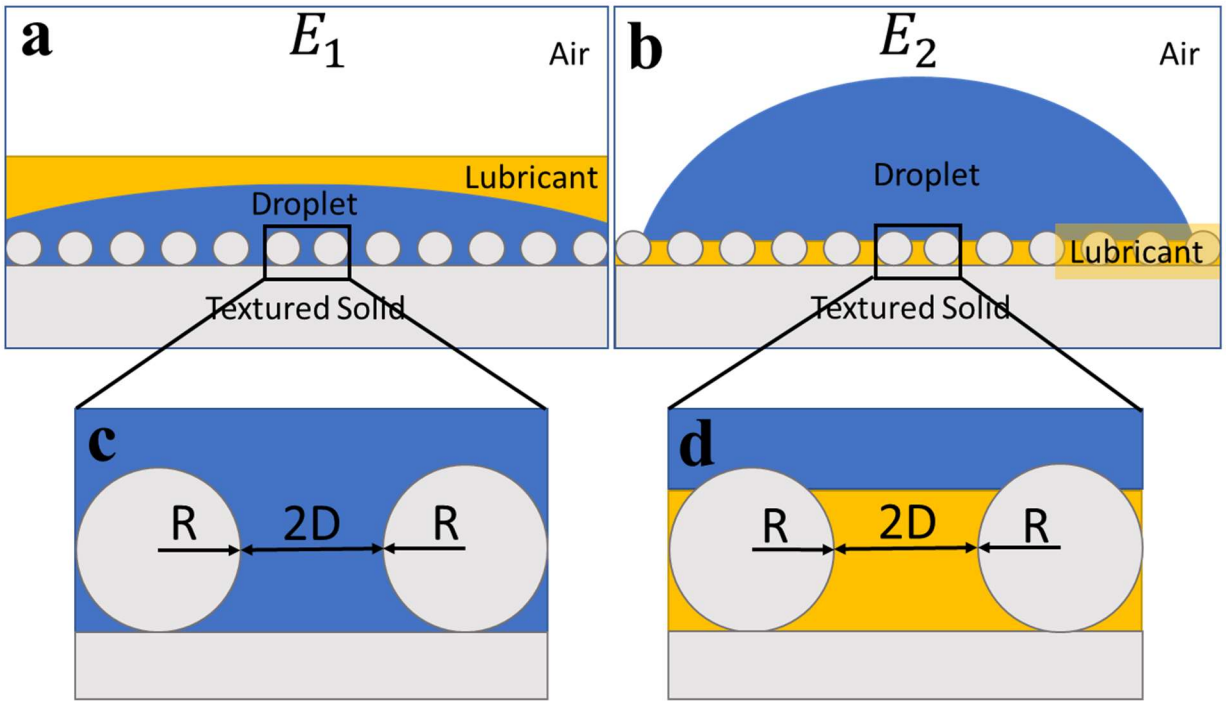

Figure 2.3*: Wetting states on LIPS on cellulose fibers. Wetting and mobility on a LIPS surface depends on the relative position and interfacial energies of the aqueous droplet, solid, and lubricant. The white area is the air. The yellow area represents the lubricant. Blue represents the droplet, and grey represents the solid texture.* ***a)*** *E_1 the droplet displaces the lubricant and wets the solid.* ***b)*** *E_2. The droplet rests on a composite layer of solid and lubricant.* ***c-d)*** *The hemp paper texture is modeled as parallel cylindrical fibers composed of cellulose of radius (R), interfeature spacing (2D), and length (L).*

We chose hemp paper as our natural material for the solid texture. Hemp paper is porous on the microscale and made of natural cellulose fibers. We modeled the hemp paper from SEM images (Figure 2.2b). In our model hemp paper is composed of set equally spaced cylindrical fibers in parallel with spacing (2D), radius (R), and length (L) (Figure 2.3a-b).

In order to determine the roughness factor (r) we defined it as:

$$r = \frac{Actual\ surface\ area\ of\ texture}{Projected\ surface\ area\ of\ texture}$$

or

$$r = \frac{A_T}{A_P} \quad \text{(Eq. 2.10)}$$

The actual surface area (A_T) of the texture is the solid-liquid interface (Figure 2.3c):

$$A_T = (2\pi \mathrm{R} + 2R + 2D)L \quad \text{(Eq. 2.11)}$$

The projected surface area (A_P) is simply surface area in the absence of texture:

$$A_P = (2R + 2D)L \quad \text{(Eq. 2.12)}$$

Thus for parallel cylindrical fibers r is:

$$r = 1 + \frac{2\pi \mathrm{R}}{(2R+2D)} \quad \text{(Eq. 2.13)}$$

Based on our SEM images (Figure 2.2b) we approximated $2\mathrm{R} = 7.6\mu\mathrm{m}$ and $2D = 34\mu\mathrm{m}$. We determined $r = 1.56$.

In E_2 there are three different regimes that must be taken into account before we can determine the energy of the state:

$$E_2 = E_{sw} + E_{so} + E_{wo} \quad \text{(Eq. 2.14)}$$

E_{so} is energy per unit area of the lubricant wetting the solid. E_{sw} is the energy per unit are of the aqueous phase wetting the solid, and E_{wo} is the interfacial energy between the lubricant and the aqueous droplet.

In order to define these terms we must first separate our roughness term. We define Φ as the solid area occluded (A_O) by the aqueous droplet divided by the projected area (A_P).

$$\Phi = \frac{Occulded\ Solid\ liquid\ area}{Projected\ Solid\ liquid\ Area}$$

$$\Phi = \frac{A_O}{A_P} \quad \text{(Eq. 2.15)}$$

The droplet will wet the solid according to Young's relation.

$$\cos\theta_{ws(o)} = \frac{\gamma_{so} - \gamma_{sw}}{\gamma_{ow}} \quad \text{(Eq. 2.16)}$$

$\theta_{ws(o)}$ is the contact angle between the aqueous phase and the solid under the lubricant phase. Since the relative position and therefore the area of the solid-aqueous interface is directly related to the position of the lubricant (Figure 2.4), we can use $\theta_{ws(o)}$ to determine the cross-sectional position of the aqueous phase and therefore the occluded area.

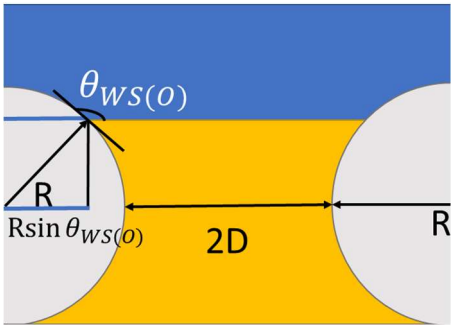

Figure 2.4: *Determining Φ for E_2 on hemp paper. The yellow area represents the lubricant. Blue represents the droplet, and grey represents the solid texture. The hemp paper texture is modeled as parallel cylindrical fibers composed of cellulose of radius (R), interfeature spacing (2D), and length (L). This figure shows the contact angle ($\theta_{ws(o)}$) between the aqueous phase and the solid cylindrical fibers under lubricant. The area of the solid occluded by the water is defined as the cross section of the cylinder at the point where the water and lubricant meet. We used geometry to determine that this line was proportional to 2R($\sin\theta_{ws(o)}$).*

From Figure 2.4, it is evident that:

$$A_O = 2\mathrm{R}(\sin\theta_{ws(o)})L \qquad \text{(Eq. 2.17)}$$

Therefore Φ can be calculated as:

$$\Phi = \frac{2\mathrm{R}(\sin\theta_{ws(o)})}{(2R+2D)} \qquad \text{(Eq. 2.18)}$$

Using the same 2R = 7.6μm and $2D$ = 34μm based on 2.2b, along with Table 2.2, we get Φ=0.09.

We can now write E_{sw} defined at just the area where the blue in Figure 2.4 touches the grey.

$$E_{sw} = \Phi^{*}\gamma_{sw} \qquad \text{(Eq. 2.19)}$$

E_{so} is only defined where the lubricant, but not the aqueious phase is in contact with the solid or where the yellow is touching grey in Figure 2.4.

$$E_{so} = (r - \Phi)^* \gamma_{so} \quad \text{(Eq. 2.20)}$$

Finally, E_{wo} is the defined along the interface between the aqueious phase and the lubricant. Since this is essiatial defined as the area where the aquious phase is not in contact with the solid, we can write this interface as:

$$E_{wo} = (1 - \Phi)^* \gamma_{so} \quad \text{(Eq. 2.21)}$$

And we can write the total equation for E_2 as:

$$E_2 = \Phi^* \gamma_{sw} + (r - \Phi)^* \gamma_{so} + (1 - \Phi)^* \gamma_{so} \quad \text{(Eq. 2.22)}$$

Using equations 2.9, 2.22, and Table 2.2 on cellulose hemp paper we get $E_1 = 0.3\text{mJ m}^{-1}$ and $E_2 = 103.6\text{mJ m}^{-1}$. Since $E_1 < E_2$, $E_1$is the favored state and droplet placed on a LIPS made from only hemp paper will displace the lubricant and wet the solid. This does not satisfy condition (iv) which states that the solid surface must be more compatible with the lubricant than water.

However, if the underlying texture were made from a hydrophobic material as opposed to a hydrophilic one, we could decrease the texture's affinity for water. Nature contains many hydrophobic waxes. We chose to coat the cellulose fibers with beeswax (Figure 2.2c) because it has already been established as a hydrophobic, edible material[36].

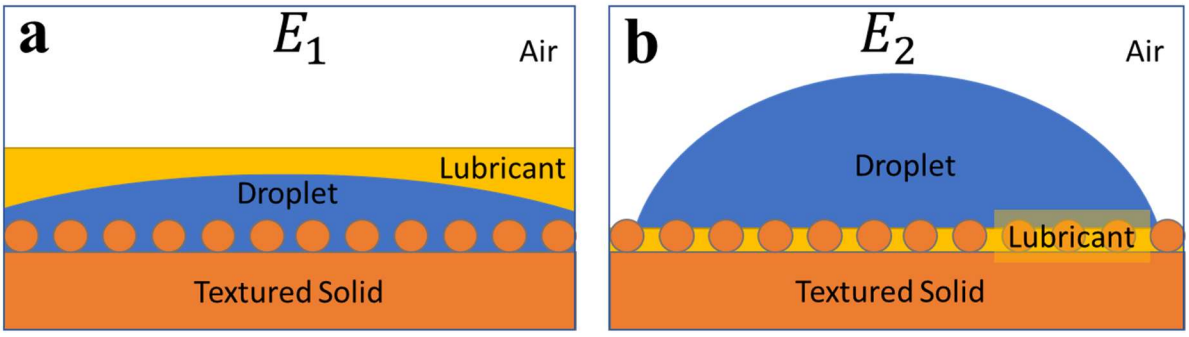

Figure 2.5: *Wetting states on LIPS on beeswax-coated cellulose fiber.* ***a)*** *$E_1$the droplet displaces the lubricant and wets the solid.* ***b)*** *E_2. The droplet rests on a composite layer of solid and lubricant*

When the fibers are coated with beeswax they are assumed to have a surface energy of 27.5mJ m^{-2}. Using the same procedure we used for cellulose fibers we determined $E_1 = 63.2$mJ m^{-2} and $E_2 = 46.8$mJ m^{-2}. Since $E_2 < E_1$, E_2 is the favored state, and droplet placed on a LIPS made from only beeswax paper should be able to sit on a composite layer of lubricant and solid and slide with minimal hysteresis at low tilt angles. Coating our paper with beeswax allows us to satisfy condition (iv).

Finally, we examine our final wetting criteria (v). The droplet should not be cloaked by the lubricant. Cloaking is where lubricant spreads completely over the outside of the droplet. This is not desirable as the removal of any droplet, regardless of any other property of the LIPS, will cause the depletion of the lubricant. Cloaking is an inherent property of the lubricant and liquid and is independent of the solid texture[11]. Therefore, we can examine the interface at the top of the droplet as shown in Figure 2.6a-b.

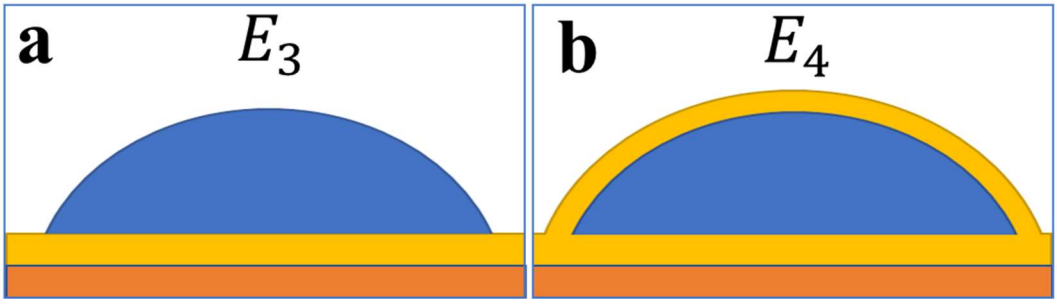

Figure 2.6: *Cloaking on a LIPS.* ***a)*** *E_3 the droplet maintains an interface between itself and the air.* ***b)*** *E_4 the droplet is cloaked by the lubricant which creates an interface with the droplet and an interface between the lubricant and air.*

E_3 is simply the surface tension of the aqueous phase.

$$E_3 = \gamma_{wv} \qquad \text{(Eq. 2.23)}$$

E_4 represents an interface where the droplet is coated by a thin layer of the lubricant. To do this the lubricant would need to form an interface completely covering the droplet represented by

γ_{wo}. Since this also forms an interface between the lubricant and the air γ_{ov}, E_4 is a combination of the two interfaces.

$$E_4 = \gamma_{wo} + \gamma_{ov} \quad \text{(Eq. 2.24)}$$

Just like before, the state with the lower energy per unit area will occur spontaneously. $E_3 = 72.8\text{mJ m}^{-2}$ and we can use the surface tension of hemp oil ($\gamma_{ov} = 32.8\text{mJ m}^{-2}$) and the interfacial energy between water and hemp oil calculated in Table 2.2 ($\gamma_{wo} = 46.7$) with Eq. 2.24 to determine that $E_4 = 79.5\text{mJ m}^{-2}$. Since $E_3 < E_4$, we can conclude that hemp oil does not cloak our droplet and satisfies criteria (v).

There are several possible objections to this model. The most obvious one being that this sort of analysis is usually conducted on ordered, predefined textures as seen with lithography and does not represent the scope of configurations that can be present in a random structure like paper. Further, the inter-fiber spacing is almost universally at angles with other fibers and is almost never seen to be parallel. Finally, the images that we take with the SEM cannot possibly account for all of the possible spacing configurations the fibers can take on.

However, there are a range of values that will enable the correct state of wetting. The variability in fiber diameter and inter-feature spacing cannot be accounted for without the totality of imaging, but we can determine where our model will break down (enter state E_1). In the case of our present model, an aqueous droplet will wet the texture if 2D > 140μm or fiber size 2R<2μm. Based on the SEM (Figure 2.2b-c) image this does not occur on the surface very often if at all. While the interfiber distance could hypothetically be that high in the case of plane paper, this is highly unlikely in the case of wax paper (Figure 2.2c). The wax coats the fibers, increasing their diameter. In some cases the wax will crystalize and completely conceal the fibers.

2.4 Fabrication of Hemp oil Infused Porous Surfaces

2.4.1 Fabricating H-HIPS

In this work, we fabricated (Figure 2.6) a hemp paper, hemp oil infused porous surface (hereafter referred to as H-HIPS). Hemp paper is composed of mostly cellulose fibers and is porous on the microscale. The fibers are naturally hydrophilic ($\gamma_{SV} = 68\text{mN m}^{-1}$)[37], so we coated them with FDA approved, natural, edible beeswax ($\gamma_{SV} = 27.5\text{mN m}^{-1}$)[35]. Then we infused the wax fibers with hemp oil ($\gamma_{LV} = 32.8\text{mN m}^{-1}$). The wax-coated hemp fibers in hemp paper act as a porous texture with a stronger affinity for the hemp lubricant oil than aqueous liquids (Chapter 2.3). We calculated E_1 and E_2 on this surface and determined that the lowest, most favorable state was E_2, and it therefore could allow aqueous liquids to slide. The fabrication procedure is shown below.

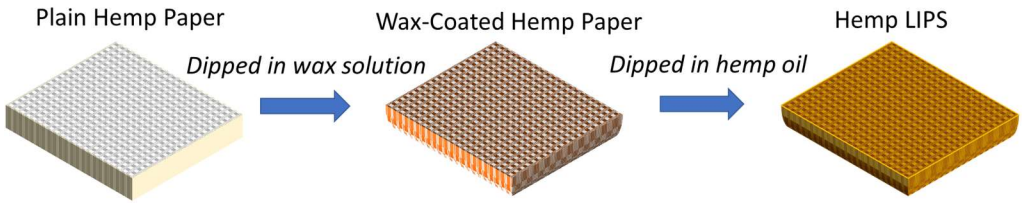

Figure 2.6: *Fabrication of hemp paper, hemp oil infused porous surface (H-HIPS).*

2.4.2 Fabricating Metallic HIPS

Many groups have used the long chain fatty acid stearic acid (C18:0)[38-40] as a means of creating hydrophobic surfaces on post-textured metals such as aluminum, copper, and steel. Hemp oil is primarily composed of long chain fatty acids (C16:2) with the essential fatty acid linoleic acid comprising half of hemp oil by mass[30,41]. We elected to modify several metallic surface directly with hemp oil for anti-icing and blood contacting applications. To our knowledge no one has fabricated a LIPS modified with the oil that is used as a lubricant.

The procedures for all fabrication of metallic HIPS are nearly identical (Figure 2.7) with minimal chemicals used for modification. We satisfy our LIPS criterial (i-v) from Chapter 1 with the following. Hemp oil is immiscible in water (i). Its low surface tension means that it will wet the metal (ii). We used acid etching create a microtexture on the metallic surfaces to satisfy criteria (iii). We modified the surfaces with hemp oil to make the surface hydrophobic ($\gamma_{SV} =$ 31.2mN m^{-1}) and more compatible with itself than water (iv). Finally, we are still using the same lubricant; so cloaking does not occur (v).

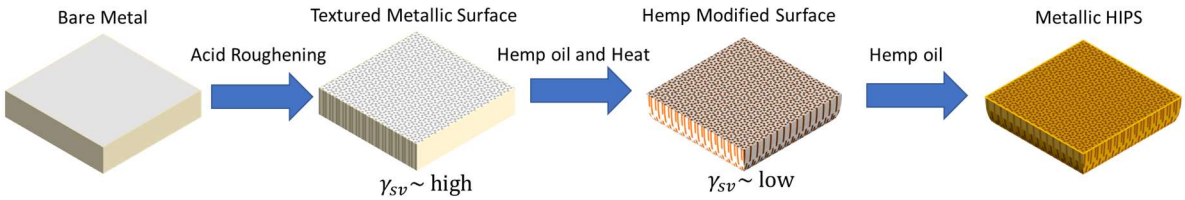

Figure 2.7: *Generalized Metallic HIPS procedure.*

2.4.2.1 Fabricating Steel HIPS

A steel sheet was boiled in 2.5 M hydrochloric acid for five minutes. The steel was then washed with water and dried with nitrogen gas. The roughened steel was then placed in a container containing pure hemp oil for 1 hr at 100°C. Sonication in acetone and ethanol was used to remove excess oil heated oil. The surface was then infused with hemp oil as the lubricant.

2.4.2.2 Fabricating Copper HIPS

Copper plates were ultrasonically cleaned in a solution of 5g NaOH, 2g Na_2CO_3, and 100 mL DI water for 10 min. Next, all samples were immersed in 5% sulfuric acid for 1 min to remove copper oxides/ then rinsed with DI water and dried with nitrogen gas. The copper plates were etched in $FeCl_3$ 5 g in 5mL DI water for 4 hours[42].

After etching, samples were rinsed with DI water then placed in a container with pure hemp oil for 1 hr at 100°C. Then the surface was sonicated in acetone and ethanol for 10 minutes

each. Then it was rinsed again with DI water and dried under nitrogen at room temperature. Finally, fresh hemp oil was infused into the surface.

2.4.2.3 Fabricating Aluminum HIPS (Al-HIPS)

Aluminum hemp infused porous surfaces (Al-HIPS) were fabricated by first cleaning aluminum sheets of 0.5mm thickness via sonication in an ethanol/acetone solution 1/1 (v/v). They were washed and dried with water. They were then submerged in a solution of hydrochloric (2 M) acid for 8-10 minutes. Finally, the aluminum was boiled for twenty minutes[43]. The aluminum was dried under N_2 then were functionalized by immersing them in hemp oil at 100ºC for 1 hr. Excess hemp oil was removed by first washing the surface with acetone and ethanol. Then the surface was sonicated in acetone and ethanol for 10 minutes each. Then it was rinsed again with DI water and dried under nitrogen at room temperature. Finally, fresh hemp oil was infused into the surface.

2.4.2.4 Fabricating Titania Nanotube HIPS (Ti-HIPS) Fabrication

Titania nanotube surfaces were fabricated by electrochemical anodization with a titanium anode and platinum cathode in a 95:2:3 DEG:HF:H2O (by volume) electrolyte at 60 V for 24 h followed by annealing in air at 530°C for 6 h. All samples were rinsed thoroughly with deionized (DI) water and dried with nitrogen.

Titanium nanotube hemp oil infused porous surfaces (Ti-HIPS) were fabricated by placing the prepared titanium nanotubes Titanium nanotubes we then exposed to oxygen plasma for 15 minutes. Then they were immediately placed in in hemp oil at 100ºC for 1 hr. Excess hemp oil was removed by first washing the surface with acetone, ethanol, and DI water. Then the surface was sonicated in acetone and ethanol for 10 minutes each. Then it was rinsed again with

DI water and dried under nitrogen at room temperature. Fresh hemp oil was infused into the surface.

2.5 Results and Discussion

2.5.1 Optimizing H-HIPS Durability

Lubricant loss is an inescapable problem with LIPS. In the case of **E₂** the surface texture acts to hold the lubricant in place via capillary forces. The smaller and more regular the texture more difficult the lubricant is to dislodge. Textures on the microscale lose lubricant more quickly with lower sheer stresses than textures with nanoscale features[42].

On H-HIPS we hypothesized that the amount of beeswax deposited on the surface would correlate to a decrease in the pore size and an increase in lubricant retention under shear stress under flow (Table 2.3).

Table 2.3: *Durability of HIPS. Top is the number of 25μL droplets run across LIP surface. Left is beeswax concentration per mL of toluene. Four trials were conducted on different parts of each surface after each number of droplets. Values are ω of 20 μL droplet. Uncertainty is standard error of the mean.*

Beeswax Concentration (mg mL^{-1})	Number of Droplets Removed from the Surface				
	200	400	1000	2000	3200
50	8.0 ± 1.0	7.6 ± 1.2	12.1 ± 0.8	17.1 ± 1.4	26.4 ± 3.8
100	7.4 ± 1.8	10.3 ± 1.4	10.5 ± 1.1	11.8 ± 1.0	21.3 ± 2.8
150	4.8 ± 0.7	7.5 ± 0.9	8.9 ± 0.6	13.5 ± 1.7	17.3 ± 2.8
200	6.5 ± 1.1	14.5 ± 5.3	33.0 ± 2.1	66.0 ± 7.8	-
600	6.7 ± 1.1	10.0 ± 2.7	16.1 ± 0.7	-	-

In order to test this we exposed our HIPS to sheer stress via the continuous application of droplets[18] (~25μL) at a low flow-rate of 1mL per minute. We tested this for wax concentrations

of 50, 100, 150, 400, and 600 (mg mL^{-1}). We then evaluated ω for each surface using a 20μL droplet. The results are shown in Table 2.3.

Based on these results we chose 150 mg/mL as the concentration of beeswax going forward, since it was able to maintain the lowest sliding angle consistently after the largest number of drops.

2.5.2 Performance of Food Sliding on H-HIPS

One application of our H-HIPS is a fully bio-degradable, non-toxic food container that can also effectively reduce food waste. Many liquid products consumed daily have lower γ_{LV} than water ($\gamma_{LV} = 72\text{mN m}^{-1}$), such as Gatorade ($\gamma_{LV} = 68\text{mN m}^{-1}$)[36], Whole Milk (49.9mN m^{-1})[44], Agave Syrup (45.3mN m^{-1})[45], Honey (32.8mN m^{-1})[46]. In order to validate that our HIPS can effectively reduce liquid waste in food containers, we tested the sliding angle (ω) of liquids with different γ_{LV} Figure 2.7. Our results indicate that liquids with at least $\gamma_{SV} > 32\text{mN m}^{-1}$ slide on our HIPS.

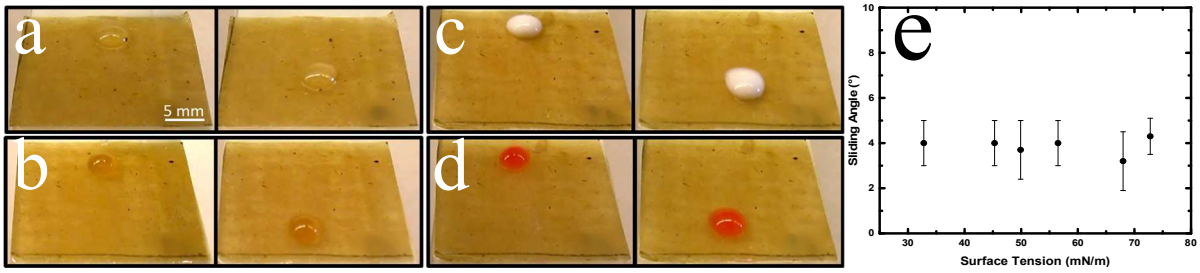

Figure 2.8: *Food liquids sliding on H-HIPS.* ***a)*** *Agave Syrup sliding* ***b)*** *Gatorade* ***c)*** *Milk* ***d)*** *dyed Water* ***e)*** *From left to right honey (32.8 mN m^{-1}), Agave Syrup (45.3 mN m^{-1}), Whole Milk (49.9 mN m^{-1}), SDS 2mM (56.5 mN m^{-1}), Gatorade (68 mN m^{-1}) Water (72.8 mN m^{-1}) .*

2.5.3 Water Sliding on Metallic HIPS

We observed near trivial sliding for water on all of our metallic HIPS (Figure 2.9). All surfaces displayed water $\theta_{adv} > 140°$ after modification with hemp oil, but before infusion indicating hydrophobicity.

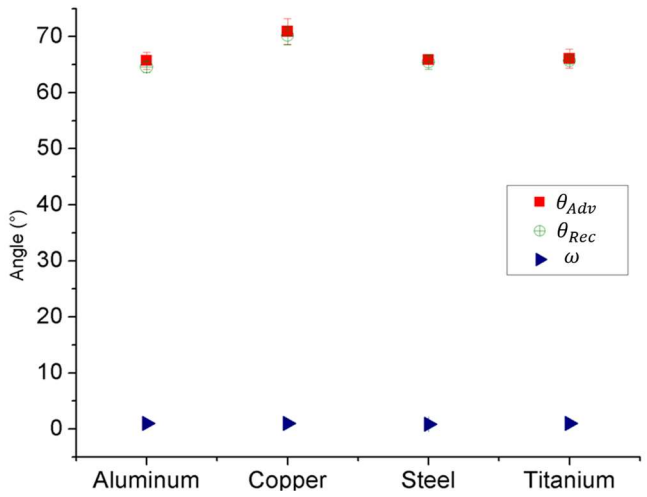

Figure 2.9: *Water sliding on metallic HIPS. Water slides off all metallic HIPS ω~1°.*

2.5.4 Anti-Icing and Deicing on Al-HIPS

In order to test anti-icing performance, we placed the Al-HIPS in a -20°C freezer. Water was chilled (T ≈ 4°C) prior to being placed on Al-HIPS droplets. These droplets were then tilted (~45°) and slid off the surface (Figure 2.10a). Droplets also slid on pre-tilted surfaces. It is also interesting to note that this phenomena was seen on one Al-HIPS made with aluminum foil as well as aluminum plate. This sliding is likely because the droplet does not become solid on the Al-HIPS. This could either be because hemp oil does not solidify at this temperature or because hemp oil impaired the transfer of heat away from the water.

Our deicing experiments indicate that ice could be trivially removed from the surface of Al-HIPS (<5kPa) through at least five cycles. This is a significant decrease in ice adhesion on bare, unmodified aluminum at -10°C which can be in excess of 1000 kPa[47]. While other LIPS reported in the past have used silicone and fluorinated oils to demonstrate de-icing and anti-icing performance, this is the first instance we are aware where a natural oil/biodegradable oil has shown anti-icing and deicing performance.

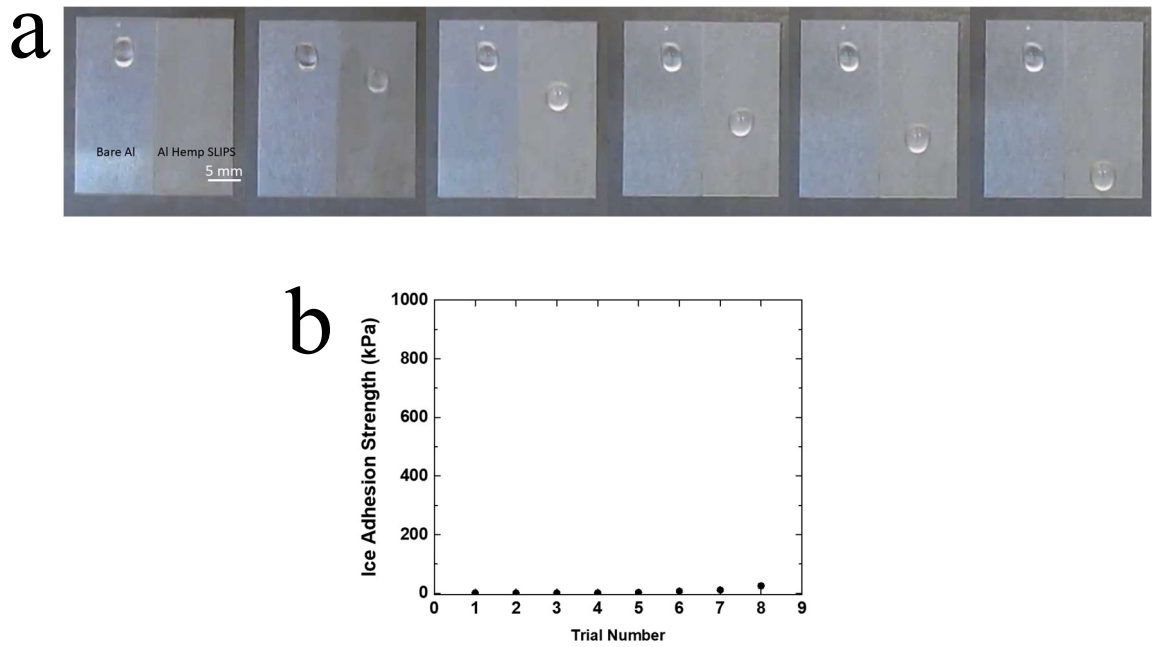

Figure 2.10: *Anti-icing performance on Al-HIPS.* ***a)*** *a droplet (T ≈ 4°C) is initially placed on a bare aluminum (Al) and Al-HIPS that have been precooled to -20°C. This shows the droplet sliding on the Al-HIPS without freezing, while the droplet adheres and ultimately freezes to the bare Al.* ***b)*** *Deicing results on Al-HIPS. Each trial represents two locations on an Al-HIP surface. Both cuvettes were filled at the same time. The cuvette that was removed first was randomized. Error bars represent standard deviation.*

2.5.5 Blood Platelet Adhesion on Ti-HIPS

The number of platelet on our Ti-HIPS (Figure 2.11c-d) was shown to be significantly less than those on bare Titanium (Ti) (Figure 2.11a) and Titanium nanotubes (NT) (Figure 2.11b). This is significant because platelet adhesion is often one of the first stages of the clotting cascade. Any blood contacting material must have some means of reducing the adhesion of platelets. Next we conducted LDH (Figure 2.11e) testing with our Ti-HIPS. Our results indicate that the Ti-HIPS are comparably cytotoxic to bare titanium which is already used in several implants.

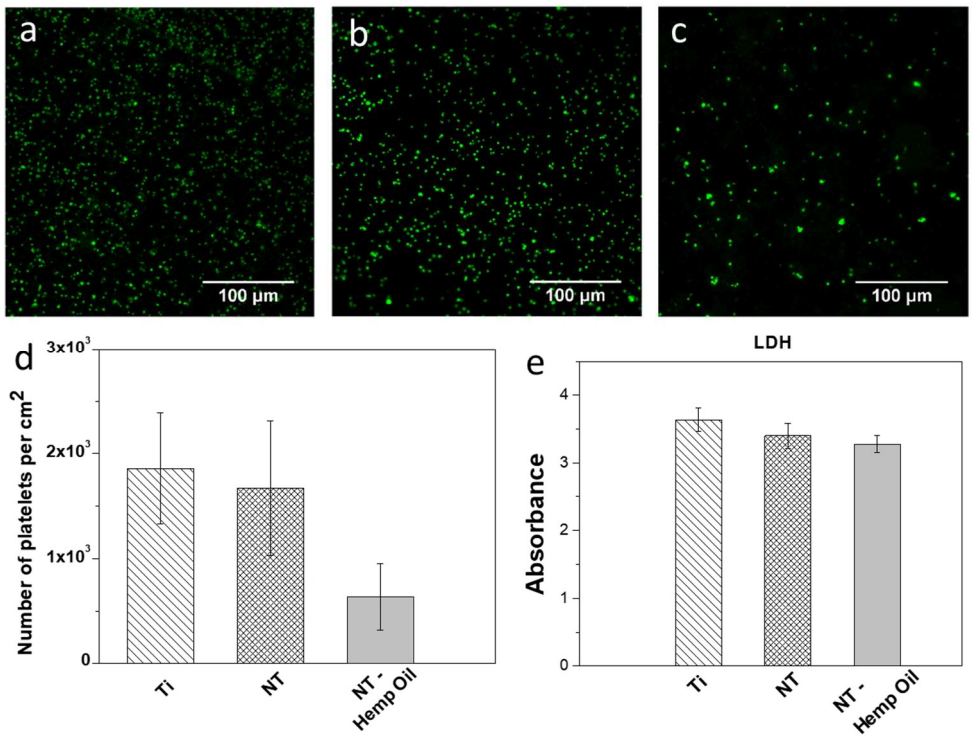

Figure 2.11: *Ti-HIPS Hemophobicity.* ***a)*** *Platelets (green) on Titanium (Ti)* ***b)*** *Platelets on Nanotubes (NT)* ***c)*** *Platelets on Ti-HIPS* ***d)*** *Platelets per unit area on Ti, NT, and Ti-HIPS* ***e)****. LDH on NT-Hemp (Ti-HIPS) has have similar cytotoxicity to bare NT. Higher values of LDH absorbance indicate increased cell death.*

2.6 Conclusion

In conclusion, we used naturally occurring hemp oil and beeswax to fabricate several LIPS with a scalable facile technique. We fabricated several with natural hydrophobic materials that exhibit low sliding angles (ω<5°) for aqueous liquids. Further, we demonstrate that food liquids with $\gamma_{LV} > 32$ mNm^{-1} display and ω <5° on our H-HIPS. We demonstrate that HIPS on aluminum is anti-icing as well as de-icing. Various metallic HIPS demonstrate extremely low sliding angle (ω~1°). Our toxicity tests based on LDH and fluorescent staining platelets indicate that Ti-HIPS fabricated with natural materials are minimally cytoxic and well as reduce platelet adhesion. Although our HIPS display reasonable mechanical durability against liquids flowing past the surface, depletion of hemp oil and pinning was eventually observed after significant

flow over the surface. However, this could easily be rectified by very small additions of hemp oil (<10μL). We envision that our methodology will have applications in reducing the waste from viscous food liquids, preventing aerospace icing, and reducing platelet adhesion.

3. Repurposing Magnetic Tapes as LIPS

3.1 Introduction

The accumulation of un-recyclable waste has become a substantial problem. Non-melt-processable plastics are polluting the environment at an alarming rate[48]. Some of these plastics contain compounds that are otherwise useful, but too expensive to reprocess[49]. Others are materials that once served a large purpose in modern technology, but have been replaced in common applications. One material that meets all of these criteria is the magnetic tape previously used in cassettes, home video recordings, and data storage,[50] which has been almost completely replaced in favor of optical disks and solid state storage.

Magnetic tapes are usually composed of two layers typically measured in the tens of microns. One is a thin a layer of magnetic micro/nanoparticles, typically ferric oxide, cobalt, or chromium, of less than five microns. The other is usually a high modulus flexible polymer such as polyethylene terephthalate (PET). The inclusion of magnetic particles makes these tapes difficult to recycle because the particles that contaminate these materials must be removed prior to the recycling. This can be accomplished with significant thermal and mechanical processing. In 2001, when these materials were more commonly manufactured and available, only 0.1 percent of all magnetic tape waste was recycled[51]. Rather than recycling the tapes, an alternative use for magnetic tapes would allow us to repurpose them for new applications.

Recently there has been a renewed interest in using thin films with bound magnetic particles as actuators to control fluid movement in microfluidic devices. These approaches have included single droplet manipulation through magneto-induced capillary forces[52], altering surface topography of gels using magnetic fields[53], and simple microcantilevers. Significant

research has been put into designing and manufacturing thin films with high magnetic density so that they can be manipulated by smaller external fields. However, these processes require special equipment and are labor intensive. Here, we show a pre-existing magnetic tapes can be repurposed as a platform for droplet manipulation. Using magnetic tape-based liquid infused porous surfaces (Mag-LIPS), simple folds and taking advantage of the stiffness of the tape, we are able to manipulate multiple droplets under gravity.

3.2 Materials and Characterization

The magnetic tape (VHS, "Fried Green Tomatoes", MCA Universal, 1992) was purchased locally. Almond oil (Sweet Almond Oil, Viva Naturals) almond oil was purchased from Amazon. A 1-inch cube neodymium (~0.5-0.6 T) permanent magnet was purchased from Applied Magnets. The magnetic tape was removed from the VHS and cut into ribbons approximately 2 cm in length. Contact angle measured using the same method discussed in section 2.2.1.

The morphology of the magnetic tape surfaces was characterized using an SEM (scanning electron microscope). Images were taken with a JEOL-6500F SEM at 15 kV at a working distance of 14.2 mm.

3.3 Designing Mag-LIP Surface

Almond oil, like most oils, is immiscible in water and has a low surface tension (28mN m^{-1})[19], so it can be assumed to wet the texture satisfying our LIPS criterias (i) and (ii) from section 1.2. SEM (Figure 3.1a) reveals that the ferric oxide side of the magnetic tape has a porous texture on the nano scale satisfying condition (iii).

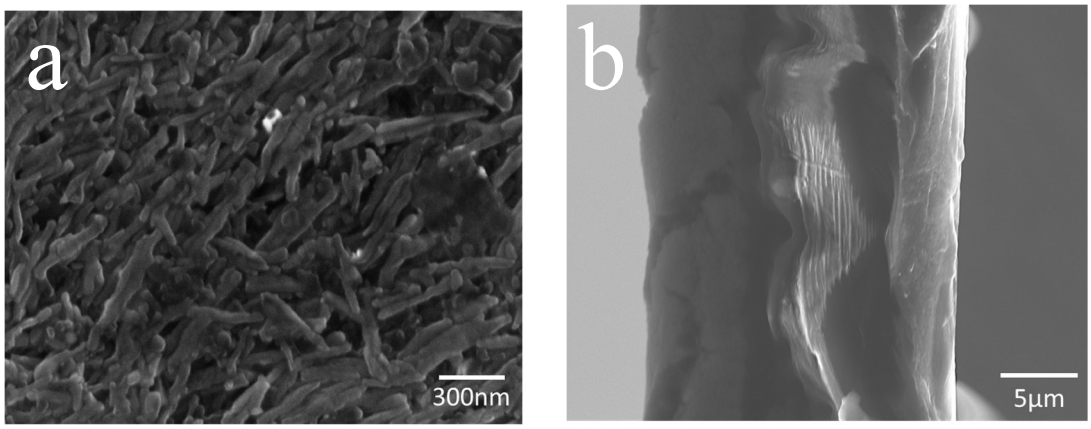

Figure 3.1: *SEM of Magnetic Tape.* ***a)*** *Cross section of magnetic VHS tape. Left side is the convex edge containing the magnetic ferric oxide. On the right is the polymer.* ***b)*** *Porous ferric oxide layer.*

Contact angle measurements on the texture give us and advancing contact angle for water $\theta_{adv} = 120$. While the contact angle for almond oil is $\theta_{adv} \sim 0$. This indicates that the almond oil is far more compatible with the solid surface than water satisfying criteria (iv). Finally, we used Eq. 2.7 to calculate $\gamma_{wo} = 46.4$mJ m^{-2}. Using Eq. 2.23-2.25 we determined $E_3 = 72.8$ and $E_4 = 74.8$. Since $E_3 < E_4$, we are able to satisfy our final criteria (v) that water is not cloaked by almond oil. Mag-LIPS were easily manufactured by infusing a thin layer of almond oil into to the iron oxide surface.

3.4 Results and Discussion

Previous reports have described magnetic tapes as bi-layered. Where one layer is composed of magnetic particles and the other is a polymer. We suspected that this layer would be composed of mostly nanoparticles in a polymer matrix. In designing a surface on top of the magnetic tape we first evaluated the tape under SEM (Figure 3.1) to determine whether there was any preexisting porous structure. This revealed that our tape was indeed bi-layered. One side is composed of iron oxide nano-texture, and the other side is a mostly featureless polymer (water $\theta_{adv} = 89.7$) which was not suitable for a LIP surface. Sliding angles for all Mag-LIP surfaces

were shown to be less than 2° for a 10µL droplet, which allowed droplets to move on the surface with minimal pinning. Droplet manipulation for both the single and multiple droplet movement are discussed in the following sections.

3.4.1 Single Droplet Manipulation

The Mag-LIPS was fixed horizontally using a plastic clip. A powerful external (~0.5-0.6 T) magnet was fixed to a non-magnetic stage and brought within 1 cm of the Mag-LIPS. Once the Mag-LIPS was horizontal, a droplet of between 10-70µL was placed on the surface. The surface was adjusted to compensate for any surface bending due to gravity, so that the droplet remained at rest. The magnet was moved up and down relative to the gravitational field (Figure 3.2).

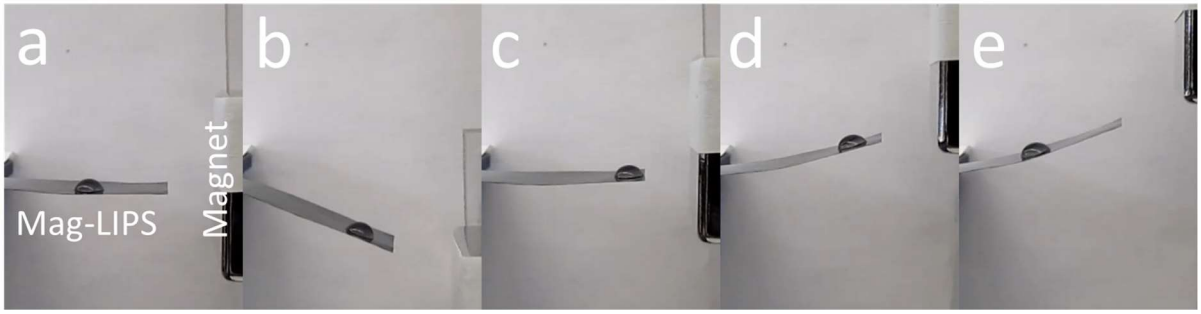

Figure 3.2: *Vertical manipulation of water droplet 20uL on Mag-LIPS.* ***a)*** *The Mag-LIPS was held at the horizontal by keeping it perpendicular to the external Magnet. A 20µL droplet was placed in the center of the Mag-LIPS.* ***b)*** *The Magnet is positioned below the horizontal. The tape bend in response to the change in the magnetic field. The droplet slides along the tape in the downward direction of the slope.* ***c)*** *The Magnet is repositioned at the horizontal. The magnetic tape the tape straightens out relative to the horizontal. The droplet stops at the edge of the tape.* ***d)*** *The Magnet is positioned above the horizontal. The tape bends upward. The droplet begins to slide down the slope in the opposite direction from (b).* ***e)*** *The Magnet height is further increased to increase the slope and therefore the sliding velocity of the droplet.*

3.4.2 Multi-Droplet Manipulation

A single piece of Mag-LIPS was cut into two equal halves down its length. These halves were placed in a perpendicular cross shape one on top of the other. The bottom of the cross was fixed to a plastic petri dish. The other half of the tape was fixed on top of the other tape with an

adhesive. After which, four droplets were placed at the outer edges of each part of the cross (labeled North, South, East, and West in Figure 3.4a). Each end of the cross was then independently manipulated by bringing the external magnet close to the Mag-LIPS in the horizontal plane. Then each section was lifted up relative to gravity until the bend in the tape was maximized.

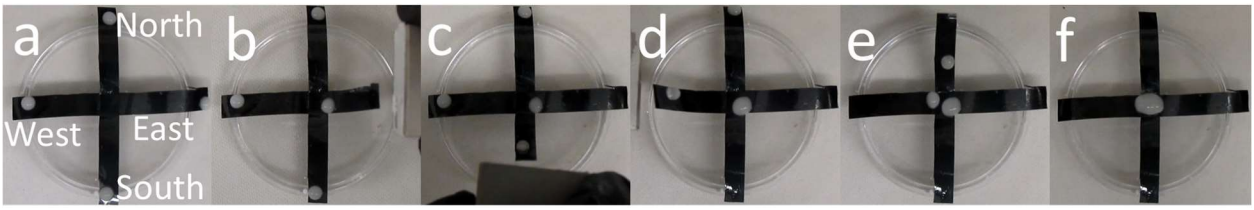

Figure 3.3: *Independent Multi-Droplet Manipulation.* ***a)*** *Four droplets of water and dilute cornstarch were 20μL each placed at the North, South, East, and West ends of two half strips of a Mag-LIPS cross.* ***b)*** *An external magnet is brought near the East end of the cross then raised against gravity until the Mag-LIPS achieves its maximum deflection. The droplet slides down the Mag-LIPS onto the center of the cross.* ***c)*** *The external magnet approaches the South end of the cross manipulates the Mag-LIPS in the same manner as (b). The droplet slides down the Mag-LIPS and coalesces with the East drop in the center of the cross.* ***d)*** *The external magnet approaches the West end of the cross manipulates the Mag-LIPS in the same manner as (b-c). The droplet slides down the Mag-LIPS and does not coalesce with the other large droplet in the center.* ***e)*** *The external magnet approaches the North end of the cross and manipulates the Mag-LIPS in the same manner as (b-d). The droplet slides down the Mag-LIPS.* ***f)*** *The South droplet coalesces with the other three droplets combining all four into a single droplet.*

3.5 Conclusion

We were able to fabricate a simple LIP surface by repurposing a magnetic tape. We were then able to bend the tape using an external magnetic field in the vertical direction. This allowed us to manipulate the motion of aqueous droplet using gravity. We also demonstrated a simple four droplet system where we could independently mix four droplets using an external magnet.

4. Future Work

4.1 All Natural Slippery Surfaces

In this work we showed a LIPS surface made entirely from natural products. However, to really demonstrate this application, it would be better to demonstrate that the wax infusion and hemp oil dip could be made to work on other paper products such as the recycled carboards that are currently used in food containers. Due to the number of times these materials have been processed they may have smaller pore sizes, so they may require less wax than the hemp paper, which is visibly rough and porous on a macro scale.

Al-HIPS show excellent promise toward a greener way to prevent the formation and adhesion of ice. However, one problem LIPS is the depletion of lubricant from external shear forces. With most commercial airliners flying at speeds in excess of 200 MPH, the shear from wind is likely very large. This might cause a near complete depletion of the lubricant. However, it is also possible that the capillary forces of the textured aluminum are able to hold the lubricant in place. Testing in real world wind situations should be done to determine if the coating is durable under real world conditions.

In our experiments we used a relatively small amount of oil to coat the surface of our Al-HIPS. However, it was visually obvious that this oil was more than enough to coat the underlying microtexture. In this vein, it will be important to establish how much oil is necessary to maintain the icephobic properties of the Al-HIPS.

Aside from problems with blood platelet adhesion, another problem implants suffer from is the adhesion of pathogenic bacteria prior to implantation. These infections are usually very serious and add additional months to the recovery time from implantation. One property of hemp

oil that has been explored in literature, but was not studied here is its anti-bacterial properties. These combined with the natural repellence of LIPS to bacteria may give implants infused with Ti-HIPS surfaces a major advantage over traditional implants.

4.2 Repurposed Magnetic Tapes as LIPS

In this work, we briefly explored the folding the tape as a means of creating channels and unique bending behavior. Subsequent work should expand upon this idea. There have been several studies done on the folding of thin magnetic actuators in order to achieve specific mechanical functions. This tape could potentially be used to manufacture grippers that apply mechanical force in the presence of a magnetic field. These grippers could be used to "pick up" droplets on superhydrophobic/superomniphobic surfaces.

4.3 Dual-phobic Surfaces from Hemp

One additional aspect of Al-HIPS that was not discussed in that section was the time necessary to modify an acid etched surface. Initial modification was done based on prior protocols using steric acid. One hour was sufficient to lower the surface energy to roughly that of hemp oil with a small polar component from Al to make the surface hydrophobic and perfect for our Al-HIPS. However, we found that if we decreased the reaction time the polar surface energy could be increased, likely due to incomplete grafting of the fatty acids to the Al surface. By tuning the time down to one minute at the same reaction temperature, we were able to achieve a surface with both underwater-superoleophobic properties and underoil-superhydrophobic properties. These regimes were once thought to be mutually exclusive.

References

1 Young, T. in *Soc. Lond.* 65-87.

2 Nishino, T., Meguro, M., Nakamae, K., Matsushita, M. & Ueda, Y. The lowest surface free energy based on− CF3 alignment. *Langmuir* **15**, 4321-4323 (1999).

3 Schrader, M. E. Wettability of clean metal surfaces. *Journal of colloid and interface science* **100**, 372-380 (1984).

4 Drelich, J., Chibowski, E., Meng, D. D. & Terpilowski, K. Hydrophilic and superhydrophilic surfaces and materials. *Soft Matter* **7**, 9804-9828 (2011).

5 Good, R. J. Contact angle, wetting, and adhesion: a critical review. *Journal of adhesion science and technology* **6**, 1269-1302 (1992).

6 Eral, H. B., 't Mannetje, D. J. C. M. & Oh, J. M. Contact angle hysteresis: a review of fundamentals and applications. *Colloid and Polymer Science* **291**, 247-260, doi:10.1007/s00396-012-2796-6 (2013).

7 Wong, T. S. *et al.* Bioinspired self-repairing slippery surfaces with pressure-stable omniphobicity. *Nature* **477**, 443-447 (2011).

8 Van Buren, T. & Smits, A. J. Substantial drag reduction in turbulent flow using liquid-infused surfaces. *Journal of Fluid Mechanics* **827**, 448-456 (2017).

9 Liu, Y., Wexler, J. S., Schönecker, C. & Stone, H. A. Effect of viscosity ratio on the shear-driven failure of liquid-infused surfaces. *Physical Review Fluids* **1**, 074003 (2016).

10 Smith, J. D. *et al.* Droplet mobility on lubricant-impregnated surfaces. *Soft Matter* **9**, 1772-1780 (2013).

11 Anand, S., Paxson, A. T., Dhiman, R., Smith, J. D. & Varanasi, K. K. Enhanced condensation on lubricant-impregnated nanotextured surfaces. *ACS nano* **6**, 10122-10129 (2012).

12 Rungraeng, N., Yoon, S. H., Li, Y. & Jun, S. Development of a self-slippery liquid-infused porous surface (SLIPS) coating using carbon nanotube composite for repelling food debris and microbial biofilms. *Transactions of the ASABE* **58**, 861-867 (2015).

13 Wang, P., Zhang, D. & Lu, Z. Slippery liquid-infused porous surface bio-inspired by pitcher plant for marine anti-biofouling application. *Colloids and Surfaces B: Biointerfaces* **136**, 240-247 (2015).

14 Qiu, R. *et al.* Fabrication of slippery liquid-infused porous surface based on carbon fiber with enhanced corrosion inhibition property. *Colloids and Surfaces A: Physicochemical and Engineering Aspects* **453**, 132-141 (2014).

15 Liu, Q. *et al.* Durability of a lubricant-infused Electrospray Silicon Rubber surface as an anti-icing coating. *Applied Surface Science* **346**, 68-76 (2015).

16 Liu, B. *et al.* Strategies for anti-icing: low surface energy or liquid-infused? *RSC Advances* **6**, 70251-70260 (2016).

17 Wang, P. *et al.* Slippery liquid-infused porous surfaces fabricated on aluminum as a barrier to corrosion induced by sulfate reducing bacteria. *Corrosion Science* **93**, 159-166 (2015).

18 Awad, T. S., Asker, D. & Hatton, B. D. Food-Safe Modi fi cation of Stainless Steel Food-Processing Surfaces to Reduce Bacterial Bio fi lms. *ACS Applied Materials & Interfaces* **10**, 22902-22912 (2018).

19 Chen, L., Geissler, A., Bonaccurso, E. & Zhang, K. Transparent slippery surfaces made with sustainable porous cellulose lauroyl ester films. *ACS Applied Materials and Interfaces* **6**, 6969-6976 (2014).

20 Steenland, K., Fletcher, T. & Savitz, D. A. Epidemiologic evidence on the health effects of perfluorooctanoic acid (PFOA). *Environmental health perspectives* **118**, 1100-1108 (2010).

21 Glavan, A. C. *et al.* Omniphobic "rFpaper" produced by silanization of paper with fluoroalkyltrichlorosilanes. *Advanced Functional Materials* **24**, 60-70 (2014).

22 Manna, U. *et al.* Slippery Liquid-Infused Porous Surfaces that Prevent Microbial Surface Fouling and Kill Non-Adherent Pathogens in Surrounding Media: A Controlled Release Approach. *Advanced Functional Materials* **26**, 3599-3611 (2016).

23 Sotiri, I., Overton, J. C., Waterhouse, A. & Howell, C. Immobilized liquid layers: A new approach to anti-adhesion surfaces for medical applications. *Experimental Biology and Medicine* **241**, 909-918 (2016).

24 Masoudi, A., Irajizad, P., Farokhnia, N., Kashyap, V. & Ghasemi, H. Antiscaling Magnetic Slippery Surfaces. *ACS applied materials & interfaces* **9**, 21025-21033 (2017).

25 Irajizad, P., Hasnain, M., Farokhnia, N., Sajadi, S. M. & Ghasemi, H. Magnetic slippery extreme icephobic surfaces. *Nature communications* **7**, 13395 (2016).

26 van der Werf, H. M. & Turunen, L. The environmental impacts of the production of hemp and flax textile yarn. *Industrial Crops and Products* **27**, 1-10 (2008).

27 Montserrat-De La Paz, S., Marín-Aguilar, F., García-Giménez, M. D. & Fernández-Arche, M. A. Hemp (Cannabis sativa L.) seed oil: Analytical and phytochemical

characterization of the unsaponifiable fraction. *Journal of Agricultural and Food Chemistry* **62**, 1105-1110 (2014).

28 Ranalli, P. & Venturi, G. Hemp as a raw material for industrial applications. *Euphytica* **140**, 1-6 (2004).

29 Ingrao, C. *et al.* Energy and environmental assessment of industrial hemp for building applications: A review. *Renewable and Sustainable Energy Reviews* **51**, 29-42 (2015).

30 Yu, L. L., Zhou, K. K. & Parry, J. Antioxidant properties of cold-pressed black caraway, carrot, cranberry, and hemp seed oils. *Food Chemistry* **91**, 723-729 (2005).

31 Beemer, D. L., Wang, W. & Kota, A. K. Durable gels with ultra-low adhesion to ice. *Journal of Materials Chemistry A* **4**, 18253-18258 (2016).

32 Movafaghi, S. *et al.* Hemocompatibility of superhemophobic titania surfaces. *Advanced healthcare materials* **6**, 1600717 (2017).

33 Owens, D. K. & Wendt, R. Estimation of the surface free energy of polymers. *Journal of applied polymer science* **13**, 1741-1747 (1969).

34 Westerlind, B. S. & Berg, J. C. Surface energy of untreated and surface-modified cellulose fibers. *Journal of Applied Polymer Science* **36**, 523-534 (1988).

35 Boyd, L. M. *Superhydrophobic surfaces for reducing liquid adhesion and contact time*, Colorado State University, (2017).

36 Wang, W. *et al.* Superhydrophobic coatings with edible materials. *ACS applied materials & interfaces* **8**, 18664-18668 (2016).

37 Westerlind, B. S. *et al.* Surface-Energy of Untreated and Surface-Modified Cellulose Fibers. *Journal of Applied Polymer Science* **36**, 523-534 (1988).

38 Zang, D. *et al.* Stearic acid modified aluminum surfaces with controlled wetting properties and corrosion resistance. *Corrosion Science* **83**, 86-93 (2014).

39 Huang, Y., Sarkar, D. K. & Chen, X.-G. A one-step process to engineer superhydrophobic copper surfaces. *Materials letters* **64**, 2722-2724 (2010).

40 Wang, Q., Zhang, B., Qu, M., Zhang, J. & He, D. Fabrication of superhydrophobic surfaces on engineering material surfaces with stearic acid. *Applied Surface Science* **254**, 2009-2012 (2008).

41 Kriese, U., Lee, C., Kim, H. & Nam, Y. Oil content, tocopherol composition and fatty acid patterns of the seeds of 51 Cannabis sativa L. genotypes. *Euphytica* **137**, 339-351 (2004).

42 Bahrami, H. T., Ahmadi, B. & Saffari, H. Preparing superhydrophobic copper surfaces with rose petal or lotus leaf property using a simple etching approach. *Materials Research Express* **4**, 055014 (2017).

43 Yang, J. *et al.* Superoleophobic textured aluminum surfaces. *New Journal of Chemistry* **35**, 2422-2426 (2011).

44 Handojo, A., Zhai, Y., Frankel, G. & Pascall, M. A. Measurement of adhesion strengths between various milk products on glass surfaces using contact angle measurement and atomic force microscopy. *Journal of Food Engineering* **92**, 305-311 (2009).

45 Soto, J. L. M., González, J. V., Nicanor, A. B. & Ramírez, E. G. R. Enzymatic production of high fructose syrup from Agave tequilana fructans and its physicochemical characterization. *African Journal of Biotechnology* **10**, 19137-19143 (2011).

46 Oroian, M. Measurement, prediction and correlation of density, viscosity, surface tension and ultrasonic velocity of different honey types at different temperatures. *Journal of Food Engineering* **119**, 167-172 (2013).

47 Sojoudi, H., Wang, M., Boscher, N., McKinley, G. & Gleason, K. Durable and scalable icephobic surfaces: similarities and distinctions from superhydrophobic surfaces. *Soft matter* **12**, 1938-1963 (2016).

48 Andrady, A. L. Assessment of environmental biodegradation of synthetic polymers. *Journal of Macromolecular Science, Part C: Polymer Reviews* **34**, 25-76 (1994).

49 Hatzikelis, C., Madonia, C. & Cosentino, C. C. (Google Patents, 1985).

50 Nikles, S. M., Piao, M., Lane, A. M. & Nikles, D. E. Ethyl lactate: a green solvent for magnetic tape coating. *Green Chemistry* **3**, 109-113 (2001).

51 Kang, H.-Y. & Schoenung, J. M. Electronic waste recycling: A review of US infrastructure and technology options. *Resources, Conservation and Recycling* **45**, 368-400 (2005).

52 Chen, H. *et al.* Ultrafast water harvesting and transport in hierarchical microchannels. *Nature materials* **17**, 935 (2018).

53 Nanni, G. *et al.* Microfabrication of magnetically actuated PDMS–Iron composite membranes. *Microelectronic Engineering* **98**, 607-609 (2012).